Chapter 4

Active bidirectional transport of vesicles on microtubules

4.1 Introduction

The network of actin and microtubule filaments serve as tracks for motor protein assisted transport of cargo vesicles and organelles from one specific location to another [1, 2, 3]. This transport process is active: multiple motor proteins bind to the filaments and the vesicles, and utilize ATP hydrolysis to convert the stored chemical energy into mechanical work [2, 4]. A certain class of motors, such as dyenin and kinesin, are processive, meaning that after attaching to the filament they hydrolyse multiple ATPs before detaching from the filament. The motors undergo a series of mechanochemical cycles, during which they attach to the filament track and undergo conformational changes driven by ATP hydrolysis. This propels the motor along specific directions along the filament, in the process dragging the attached cargo along with it [5]. The filaments are polar, with one end of the filament chemically and morphologically different from the other [5, 6]. The motors recognize the polarity of the filament to which they bind and move in a directional way. Kinesin and dyenin family of motors translate along microtubule filaments, with the kinesin moving towards the plus end of the track [7] and dyenin exhibiting minus-end directed motion [8]. Myosin family of motors move exclusively on actin filaments [9, 10]. Usually the transport of a single vesicle is not only performed by many motors together, but different types of motors attach to the cargo simultaneously [2, 3, 11, 12, 13].

In this chapter, we will focus on vesicle transport along microtubules. Biochemical and biophysical experiments using optical traps [14] and single-molecule fluorescence imaging [15, 16] have been able to shed light on the key players, the regulatory mechanism and the dynamics of this elaborate transport system.

Most long range directed transport of vesicles and organelles is done on microtubules [17, 18]. Typically the microtubules are radially organized in a cell, such that their minus ends are clustered around the microtubule organizing center (MTOC) in the vicinity of the cellular nucleus and the plus ends pointing towards the periphery of the cell [2, 6, 18].

Recent single particle tracking experiments reveal that transport of vesicles is done bidirectionally along the microtubules [11, 18, 19]. Bidirectional motion of the vesicle, as opposed to unidirectional motion, is ‘saltatory’, characterized by the fact that the vesicles move in a specific direction, then halt and change their direction [2]. In this chapter, we develop a model for bidirectional transport of vesicles driven by multiple, processive motors of different types. In this model, the state of the vesicle is described by the number of plus-end directed motors (kinesin) and minus-end directed motors (dyenin) carried by the vesicle

cargo that are attached to the filament. We write down the general master equation governing the time evolution of the state of the vesicle. Next we consider microscopic models for the form of the velocity of the vesicle and the (un)binding rates of the motors in a given state. With these inputs we determine the steady state solutions of the master equation and subsequently determine various macroscopic transport properties such as the (i) distribution of the velocity of the vesicles, (ii) distribution of reversal times of the vesicles, (iii) first passage time of unbinding of the vesicle from the microtubule and (iv) average number of the motors attached to the microtubule. This allows us to predict the statistics of trajectories of the vesicles which can be compared to single particle tracking experiments. The hope is that this model in conjunction with vesicle tracking experiments would be able to shed light on the microscopic mechanisms of (un)binding and movement of transport vesicles by multiple motor activity.

4.2 Bidirectional transport

Bidirectional transport is common and has been observed in various cellular contexts, e.g., mitochondria [19, 20, 21], endosomes [22], pigment vesicles [11, 18, 23, 24] and secretory vesicles [25]. We take a closer look at two such examples of bidirectional transport.

(A) Transport of mitochondria along axons

An axon is a long slender projection of a nerve cell, or neuron, that conducts electrical impulses away from the neuron's cell body. Axonal transport, is responsible for movement of mitochondria, lipids, synaptic vesicles and proteins to and from a neuron's cell body, through the cytoplasm of its axon [2]. In the neuron, mitochondria are present throughout the axon, but they move towards regions in the cell which require high ATP production. In axons, microtubules are arranged with their plus ends towards the growth cones situated in the synapse, and their minus ends towards the cell body. Mitochondria travel bidirectionally along these microtubules. Dyenin and kinesin motors move along the microtubules carrying the mitochondria. When the growth cones are active due to stimulation by nerve growth factor (NGF), then a net transport of mitochondria towards the active growth cone is seen [2, 19]. If the growth cones are arrested by stopping NGF signalling, there is a net transport back to the cell body (Fig. 4.1). In experiments with cultured neuron cell [19], it was seen that the distribution of mitochondria in actively growing axons was highly skewed towards the growth cone, with seven fold higher density in the region immediately adjacent

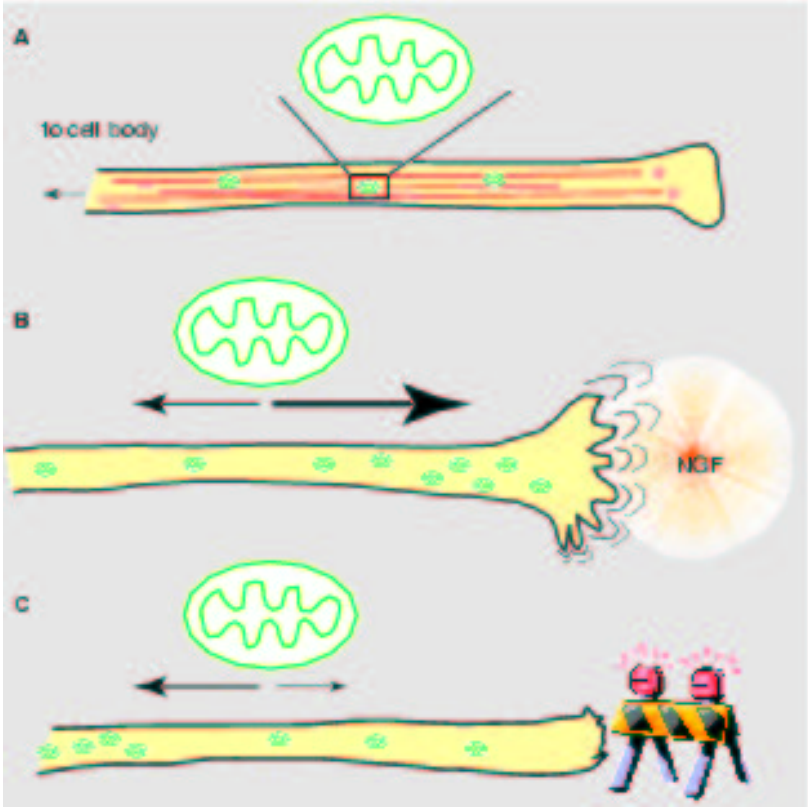

Figure 4.1: Transport of mitochondria in axons: Showing a net aggregation of mitochondria near the growth cone in the growing phase of the axon and the transition to even distribution in the absence of NGF signalling [2]

to the growth cone, than in the region 100 μm away. When axonal outgrowth was blocked, then within an hour the mitochondria distribution became uniformly distributed. Analysis of individual mitochondrial behaviour revealed that mitochondrial movement everywhere was bidirectional. Further, it was seen from individual trajectories of the mitochondria that the fraction of time spent moving anterogradely (towards the axon tip) was sharply reduced for non growing axons. The data indicated that mitochondria possess distinct motor activities for both directions of movement which was regulated for the growing and the stationary state of the axon [19].

(B) Transport of melanosomes

In melanophores (pigment cells), melanosomes are organelles containing melanin, the most common light-absorbing pigment found in the animal kingdom. In many species of fish, amphibians, crustaceans and reptiles, melanosomes can be highly mobile within the cell. In response to hormonal control, the mobility of melanosomes is regulated to attain

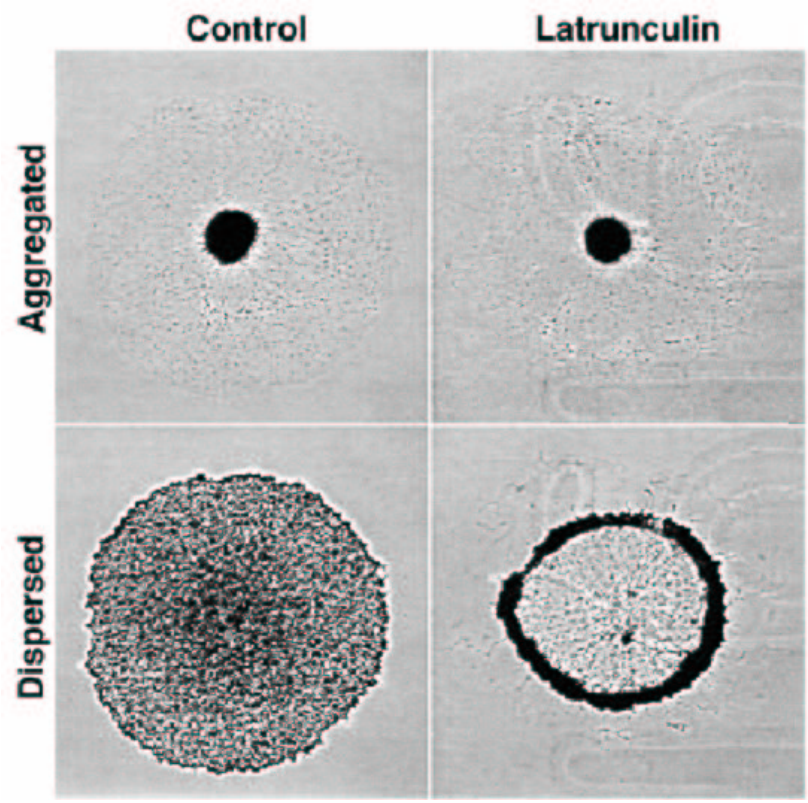

Figure 4.2: Aggregation and dispersion of pigment granules in fish melanophores: In the presence of actin, pigment granules aggregate near the cell centre or disperse throughout the cell. In the absence of actin (Latrunculin treated), the granules either aggregate near the cell centre or at the periphery in response to specific hormonal stimulus [18].

visible changes in colour. Melanophores rely on microtubule and actin based network to transport these pigment organelles. Experiments done with Xenopus (frog) melanophores and fish melanophores throw light on the complete transport machinery and the mechanism of organelle transport. These experiments [18] revealed that pigment granules either aggregated near the the cell centre or dispersed throughout the cell, in response to specific neural or hormonal stimulus. Depolymerisation of actin by Latrunculin resulted in aggregation of granules either near the cell centre or at the periphery, and the cell did not exhibit the dispersed state. This, combined with analysis of the individual trajectories of the pigment granules, revealed the role of actin and myosin, along with microtubule, dyenin and kinesin in regulating the transport of the pigment granules [18] (Fig. 4.2). In the absence of actin, it was seen that the velocity distribution of the melanosomes transported by cytoplasmic dyenin or kinesin-2, under conditions of aggregation or dispersion (Fig. 4.2), had several

peaks and could not be fitted to a single gaussian [11]. It further revealed two crucial aspects about transport and regulation of pigment granules. First, the transport of granules was performed by multiple motors of opposite kinds, i.e., plus and minus-end directed motors, and second, that hormonal signals, leading to change in the spatial distribution of granules, can be attributed to the regulation of the motor binding rates.

4.3 Single-particle model for bidirectional transport with multiple processive motors

Bidirectional transport involves vesicle transport by both types of motors, i.e., the plus-end directed motors and the minus-end directed motors. Inspite of the tendency of these motors to carry the vesicles in opposite directions, one observes long distance transport of cargoe on microtubule filaments and polarized distribution of these cellular cargo. Further, there is a robust regulatory mechanism involving the interplay of hormonal or neural stimulus with the motor binding rates. Though vesicle cargo change their direction of motion during bidirectional transport, it is able to achieve directed transport and a polarized steady state distribution by suitable regulation of the different motor's unbinding/binding rates to the microtubule [3, 11]. This control mechanism again reaffirms the theme, that the effect of specific chemical degrees of freedom associated with motor binding rates, result in the regulation of emergent macroscopic transport. The regulation mechanism for intra-cellular transport has three potential control points [2].

- Docking of motors to their cargo vesicles.
- Attachment of motors to the microtubule.
- The rate of mechanochemical cycle of the motors.

We will incorporate these mechanisms within a single-particle transition rate model. This model is a generalization of the model proposed by [26], to bidirectional transport, involving different types of motors (kinesin and dyenin). The inputs of the model involve microscopic models for the velocity and the (un)binding rates of the motors to the microtubule. We make specific qualitative and quantitative predictions of various macroscopic transport properties and statistics of vesicle trajectories, which in principle can be tested in controlled *in-vitro* experiments. Such a single-particle description of cellular cargo is appropriate only in the dilute limit, i.e., low concentration of vesicles or organelles as it does not include the effects

of loading or off-loading at the boundaries, or interaction between vesicles. In the next chapter we develop a model for vesicle transport, which incorporates the effects of interaction and finite boundaries.

4.3.1 The model

Consider a cargo vesicle transported by n dyenin motors and m kinesin motors on a single microtubule filament. These motors are irreversibly bound to the cargo vesicle but bind and unbind onto the microtubule filament along which they move. The number of dyenin motors, attached to the microtubule can vary between $n = 0$ to a maximum of $n = N$. Similarly the number of kinesin motors, attached to the microtubule can vary between $m = 0$ to a maximum of $m = M$. We will denote the state of the vesicle as $|\, n, m\rangle$. There are clearly $(N+1) \times (M+1)$ different states of the vesicle. If the cargo vesicle is in state $|\, n, m\rangle$ then it moves with a velocity $V_{n,m}$. Binding of a kinesin and dyenin motor to the microtubule occur with rates $\alpha^k_{n,m}$ and $\alpha^d_{n,m}$ respectively, while unbinding of kinesin and dyenin motors occur with rates $\beta^k_{n,m}$ and $\beta^d_{n,m}$.

First, we write the general master equation for the time evolution of the state of the cargo vesicle with a general expression for rates of binding and unbinding of the dyenin and kinesin motors. We will assume that there is no spatial dependence of the state of the vesicle cargo. Further, we will consider that the probability of simultaneous (un)binding of more than one motor to the microtubule is negligibly small.

We define,

P_{nm} = Probability of the vesicle to be in state $|n, m\rangle$

α^k_{nm}= Kinesin binding rate in state $|\, n, m\rangle$

α^d_{nm}= Dyenin binding rate in state $|\, n, m\rangle$

β^k_{nm}= Kinesin unbinding rate in state $|\, n, m\rangle$

β^d_{nm}= Dyenin unbinding rate in state $|\, n, m\rangle$

The dynamics of the unbound state of the vesicle is given by,

$$\partial_t P_{00} = \beta^k_{01} P_{01} + \beta^d_{10} P_{10} - \left(\alpha^k_{00} + \alpha^d_{00}\right) P_{00}, \tag{4.1}$$

While the general evolution equation for state $|\, n, m\rangle$ is given by,

$$\begin{aligned} \partial_t P_{nm} &= \beta^d_{n+1,m} P_{n+1,m} + \beta^k_{n,m+1} P_{n,m+1} + \alpha^d_{n-1,m} P_{n-1,m} + \alpha^k_{n,m-1} P_{n,m-1} \\ &- \left(\alpha^k_{nm} + \alpha^d_{nm} + \beta^k_{nm} + \beta^d_{nm}\right) P_{nm} \end{aligned} \tag{4.2}$$

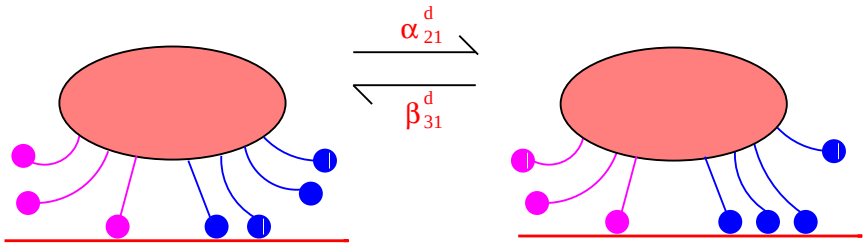

Figure 4.3: A vesicle cargo carrying 4 dyenin (N = 4) and 3 kinesin(M = 3). The cargo vesicle with 2 attached dyenin (n=2) and 1 attached kinesin (m = 1), corresponding to the state $|\,2,1\rangle$ can reversibly transform to a state with 3 attached dyenin and 1 attached kinesin, corresponding to state $|\,3,1\rangle$. Dyenin (kinesin) motors are depicted in blue (pink).

In the equation above, the first four terms on the right are the gain terms due to the fact that states $|\,n,m+1\rangle, |\,n,m-1\rangle, |\,n+1,m\rangle, |\,n-1,m\rangle$ can transform into $|\,n,m\rangle$, with rates specified by the respective (un)binding rates of kinesin and dyenin in those states from which it transforms. The next four terms are the loss terms due to the fact that $|\,n,m\rangle$ can transform to states, $|\,n,m+1\rangle, |\,n,m-1\rangle, |\,n+1,m\rangle, |\,n-1,m\rangle$ with (un)binding rates of dyenin and kinesin in state $|\,n,m\rangle$. (Fig. 4.3) shows an example of how a particular state of the vesicle can change into another.

4.3.2 Steady state

To determine the transport properties of the bound vesicle cargo in its steady state we look at the stationary solution of the master equation, i.e., $\partial_t P_{n,m} = 0$ for all n, m. We are interested in those steady states that satisfy detailed balance. It is simple to realize the condition of detailed balance in the case when the binding sites of two different kinds of the motors are well separated so that binding/unbinding rates of dyenin and kinesin are decoupled from one another. The detailed balance condition for each state $|\,n,m\rangle$ implies (Fig. 4.4):

$$P_{nm} = \prod_{i=0}^{n} \prod_{j=0}^{m} D_i K_j P_{00} \tag{4.3}$$

where $D_0 = 1, K_0 = 1$, and

$$\begin{aligned} \frac{\alpha^d_{i-1,0}}{\beta^d_{i,0}} = \frac{\alpha^d_{i-1,1}}{\beta^d_{i,1}} \cdots = \frac{\alpha^d_{i-1,m}}{\beta^d_{i,m}} = \cdots = \frac{\alpha^d_{i-1,M}}{\beta^d_{i,M}} \equiv D_i \\ \frac{\alpha^k_{0,j-1}}{\beta^k_{0,j}} = \frac{\alpha^k_{1,j-1}}{\beta^k_{1,j}} \cdots = \frac{\alpha^k_{n,j-1}}{\beta^k_{n,j}} = \cdots = \frac{\alpha^k_{N,j-1}}{\beta^k_{N,j}} \equiv K_j \end{aligned} \tag{4.4}$$

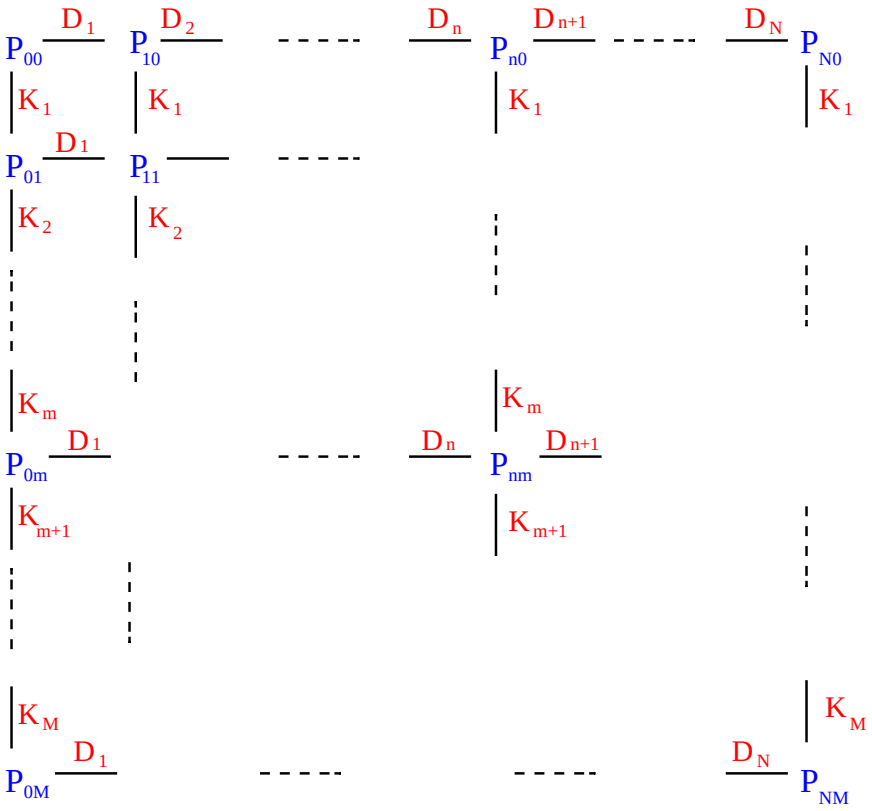

Figure 4.4: Shows the structure of how the distribution function of the states are related with each other in terms of rate constants D_i, K_j when the dyenin binding/unbinding rates are decoupled from kinesin.

Equation (4.4) is the formal way of stating that the dyenin (un)binding rates, are independent of kinesin (un)binding rates, so that the rate constants D_i, K_j are independent of each other. With the normalization condition,

$$\sum_{i=0}^{N}\sum_{j=0}^{M} P_{00} = 1, \tag{4.5}$$

we find that,

$$P_{00} = \left[\sum_{n=0}^{N}\sum_{m=0}^{M}\prod_{i=0}^{n}\prod_{j=0}^{m} D_i K_j\right]^{-1} \tag{4.6}$$

Thus given the rate constants of dyenin and kinesin in different states, one can completely obtain the steady state distribution of the various states of the vesicle, P_{nm} using equation (4.3).

4.3.3 Modeling velocity and (un)binding rates

In order to evaluate various transport properties, we need to specify the dependences of the (un)binding rates and the velocity of the vesicle on the number of attached dyenin and kinesin motors.

(i) **(Un)binding rates: dilute motor coverage** [26]

The condition of detailed balance stated above is valid when the (un)binding rates of dyenin and kinesin motors are taken to be independent of one another. We now make a further simplifying assumption of dilute motor coverage, i.e., for every motor, the binding sites on the vesicle surface are well separated and non-interacting. Then,

$$\begin{aligned} \alpha_{nx} &= (N-n)\alpha_d \qquad \beta_{nx} = n\beta_d \\ \alpha_{xm} &= (N-m)\alpha_k \qquad \beta_{nx} = m\beta_k \end{aligned} \tag{4.7}$$

where α_d, β_d are the binding and unbinding rates for a single dyenin motor and α_k, β_k are the binding and unbinding rates for a single kinesin motor [26]. This additional simplification leads to the following rate constants,

$$\begin{aligned} D_i &= \frac{(N-i+1)}{i}\left(\frac{\alpha_d}{\beta_d}\right) \\ K_j &= \frac{(M-j+1)}{j}\left(\frac{\alpha_k}{\beta_k}\right) \end{aligned} \tag{4.8}$$

Specifying these parameters enables us to find the expression for the steady state probability distribution function, P_{nm}.

(ii) **Velocity of vesicle**

The state of the vesicle depends on the number of attached dyenin and kinesin, (n,m). In order to make connection with experiments studying vesicle trajectories, we have to assume a microscopic model for the velocity of the vesicle. We propose three models for the velocity of the vesicle

Model A: The velocity of the vesicle is proportional to the difference in the number of attached dyenin and kinesin motors, thus,

$$V_{nm} = V_o\,(m-n) \tag{4.9}$$

This ansatz leads to a 'tug-of-war', where the direction of transport of the vesicle is determined by the difference between the number of the two types of motors, each type trying to pull in a specific direction. This model also implies that when the difference in number of each type of motors is zero, the vesicle does not move at all. Thus we inherently assume that the pulling strength and velocity of single dyenin is the same as that of a single kinesin. This is consistent with the results of certain *in-vitro* experiments on vesicle transport [18]. Our subsequent results and plots are obtained with this model.

The other two models that we consider, invoke a self regulatory mechanism, wherein the *regulatory switch* activating only one class of motors, depends on the number of attached motors. It is worthwhile mentioning that apart from these self-regulatory mechanism there might exist many external regulatory mechanisms to ensure the active engagement of one type of motor to the filament, while turning off the other motor [2, 3]. Models which incorporate self regulation are,

Model B [26]:

$$\begin{aligned} V_{nm} &= V_1 \qquad if \;\; n > m \\ V_{nm} &= V_2 \qquad if \;\; n < m \end{aligned} \tag{4.10}$$

where, V_1 and V_2 are constants.

Model C: There is a linear dependence of the velocity on the number of attached motors of one type,

$$\begin{aligned} V_{nm} &= nV_1 \qquad if \;\; n > m \\ V_{nm} &= mV_2 \qquad if \;\; n < m \end{aligned} \tag{4.11}$$

where, V_1 and V_2 are constant with opposite signs.

Once we have specified these microscopic transport mechanisms, we can make specific predictions about the macroscopic trajectories of the vesicles based on our model. We will see later in this section, how analysing the macroscopic trajectories of the vesicles can provide some information about the underlying microscopic transport mechanisms.

Our model has five independent parameters; $\alpha_k, \beta_k, \alpha_d, \beta_d$ and V_o which can be estimated from the study of single motor dynamics. From studies of single kinesin motors, we take

$\alpha_k = 5\ s^{-1}$ [27] and $\beta_k = 1\ s^{-1}$ [28, 29]. We also look at perturbations of these parameters by specific hormonal signalling [19]. Further, within each family of motors, there are different variants with different (un)binding rates. From studies of single dyenin motors, we take $\beta_d = 0.2\ s^{-1}$ [30] and $\alpha_d = 0.04\ s^{-1}$ [31]. The parameter V_o , the speed of the vesicle carried by a single dyenin or a single kinesin is taken to be $1\mu m/s$ [18]. Apart from making comparisons with *in-vitro* experiments on vesicle trajectories, we will highlight certain qualitative features that emerge from the model.

We will now focus on evaluating expressions for various transport properties which can be measured in controlled *in-vitro* experiments on cellular extracts containing pigment vesicles, dyenin and kinesin motors and microtubules. Statistical analysis of individual vesicle trajectories can be used to determine the distribution of velocities, distribution of plus-end directed, minus-end directed and stationary trajectories, the statistics of detaching and the distribution of reversal times.

4.4 Results

4.4.1 Steady state distribution of vesicles

The expression for the probability distribution function for the unbound state of the vesicle can obtained using the forms of D_i and K_j in equation (4.4),

$$P_{00} = \left[\left(1 + \frac{\alpha_d}{\beta_d}\right)^N \left(1 + \frac{\alpha_k}{\beta_k}\right)^M\right]^{-1} \tag{4.12}$$

From this relation and using equation (4.3), the probability distribution for any $|n, m\rangle$ state of the vesicle can be determined numerically.

4.4.2 Average number of bound motors

The average number of dyenin motors attached to the microtubule when the vesicle is in the bound state can be obtained from,

$$N_d = \sum_{n=0}^{N}\sum_{m=0}^{M} \frac{nP_{nm}}{1 - P_{00}} \tag{4.13}$$

Equation (4.15) leads to,

$$N_d = N\frac{\left(\frac{\alpha_d}{\beta_d}\right)\left(1 + \frac{\alpha_d}{\beta_d}\right)^{N-1}\left(1 + \frac{\alpha_k}{\beta_k}\right)^M}{\left(1 + \frac{\alpha_d}{\beta_d}\right)^N\left(1 + \frac{\alpha_k}{\beta_k}\right)^M - 1}. \tag{4.14}$$

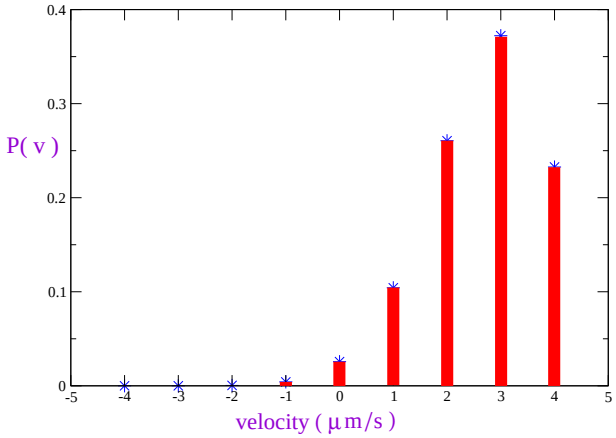

Figure 4.5: Probability distribution of the velocity of the cargo vesicles with discrete peaks at integer multiples of $V_o = 1\mu m/s$. This plot corresponds to a high duty cycle ratio for kinesin with $\frac{\alpha_k}{\beta_k} = 5$ and a low duty cycle ratio for dyenin with $\frac{\alpha_d}{\beta_d} = 0.2$. In this plot, $N = M = 4$.

In the limit $N \gg 1$, this expression reduces to,

$$N_d = N\frac{\left(\frac{\alpha_d}{\beta_d}\right)}{\left(1 + \frac{\alpha_d}{\beta_d}\right)} = NQ_d, \tag{4.15}$$

where Q_d is the duty ratio of a single dyenin attaching to the microtubule. Thus we see that multiple motors effectively increase the duty ratio for binding. Similarly the average number of bound kinesin motors or total number of bound motors can be evaluated.

4.4.3 Velocity distribution

The distribution of the velocity of vesicles can be obtained by summing weights of those states for which $n - m$ is the same. We do it numerically using the models of velocity described in section (4.3.3). When the binding rate constant for kinesin is very large compared to dyenin, then the distribution of the velocity is heavily skewed towards the positive values (Fig. 4.5). When the binding rate constants for both dyenin and kinesin motors are the same, then we have a symmetric distribution of the velocity of the vesicle, with no net transport in either direction (Fig. 4.6). We predict that the fraction of trajectories which are stationary, decreases with the relative increase of binding rate constant for one type of motor compared to the other. Fig. 4.7 shows the distribution of the velocity of vesicles obtained in *in-vitro* studies [11]. These authors [11] study the distribution of vesicle trajectories, by separating

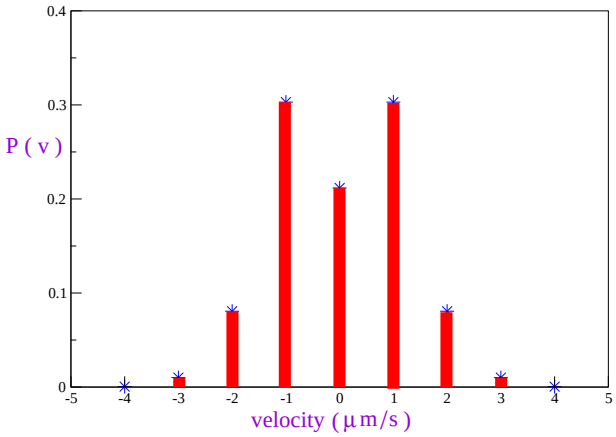

Figure 4.6: Probability distribution of the velocity of the cargo vesicles with discrete peaks at integer multiples of $V_o = 1\mu m/s$. This plot corresponds to equal duty cycle ratio for both kinesin and dyenin with $\frac{\alpha_k}{\beta_k} = \frac{\alpha_k}{\beta_k} = 0.2$. In this plot $N = M = 4$.

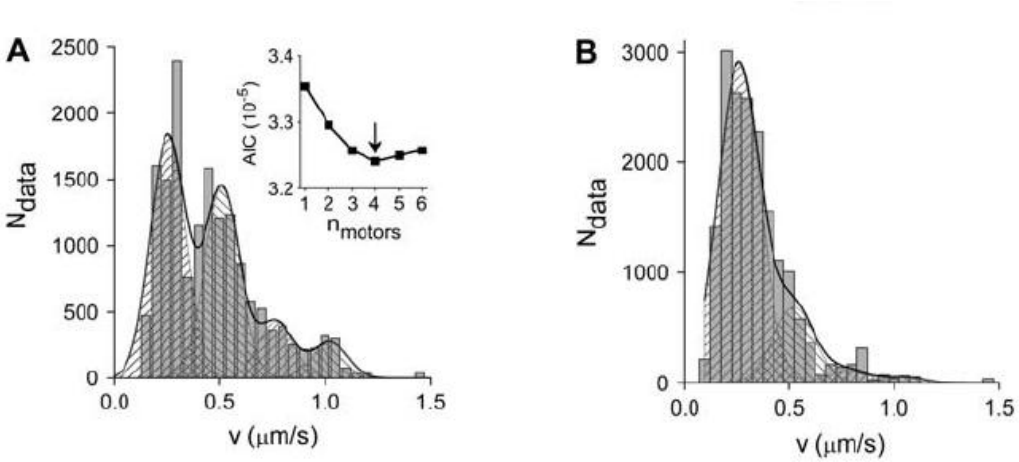

Figure 4.7: Velocity distribution of melanosomes from experiments [11]. (A) The distribution obtained from the minus end directed trajectory. (B) The distribution obtained from plus end directed trajectory. Note the discrete peaks occuring at integer multiple of $V_o = 0.25$ $\mu m/s$.

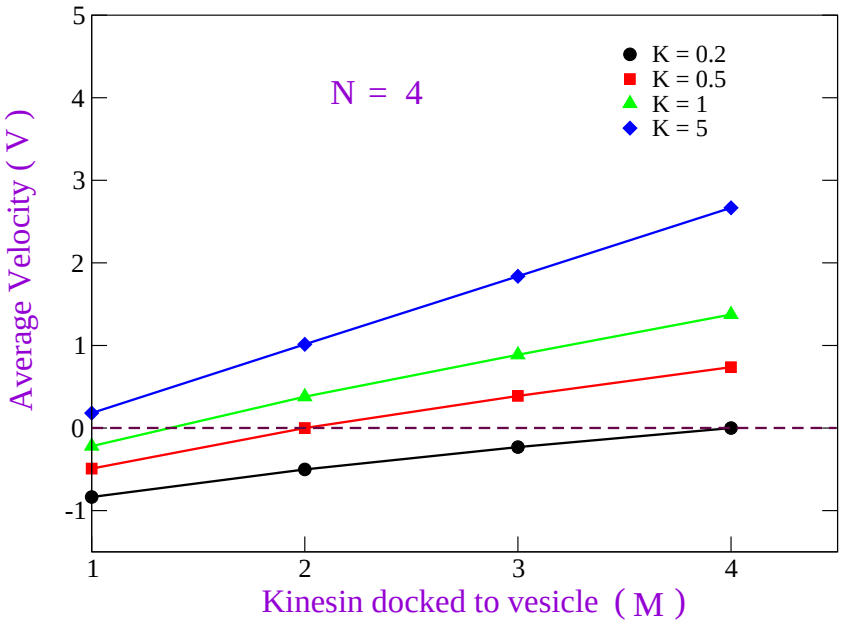

Figure 4.8: Variation of the average velocity of the vesicle cargo with increasing number of kinesin motors carried by the vesicle (M), keeping the maximum number of dyenin, ($N = 4$) the same. Increasing the duty ratio of kinesin relative to dyenin leads to more plus directed run and hence an increase in average velocity of the vesicle. $D = \frac{\alpha_d}{\beta_d} = 0.2$ is fixed. As $K = \frac{\alpha_k}{\beta_k}$, the binding rate constant for a single kinesin is increased, the average velocity also increases.

out the plus-ended and the minus-ended runs of the vesicles and hence is not suitable for direct quantitative comparison with our model. The distribution of velocities obtained from the experiments, exhibits discrete peaks corresponding to integer multiples of $V_o = 0.25\mu m/s$. This would suggest that **Model B** for the vesicle velocity (section 4.3.3), is ruled out, as this would have lead to only two discrete peaks in the velocity distribution. Our **Model A** does reproduce the qualitative features of the distribution function,i.e., multiple discrete peaks. This model also exhibits the qualitative feature pertaining to trajectories of mitochondria in axonal transport. In these experiments [19], the percentage of plus-end directed trajectories is more than minus-end directed trajectories in growing axons in region far from growth cone. In non-growing axons the percentage is roughly the same for both kind of trajectories [19]. In our model we obtain similar regulatory behaviour on changing the binding rate constants for dyenin and kinesin, a feature illustrated in Fig. 4.5 and Fig. 4.6.

In our model, the expression for average velocity of the bound vesicle is given by,

$$V = V_0 \sum_{n=0}^{N} \sum_{m=0}^{M} \frac{(m-n)P_{nm}}{1-P_{00}} \tag{4.16}$$

which can be evaluated to give,

$$V = V_0 \left[M \frac{\left(\frac{\alpha_k}{\beta_k}\right)\left(1+\frac{\alpha_k}{\beta_k}\right)^{M-1}\left(1+\frac{\alpha_d}{\beta_d}\right)^{N}}{\left(1+\frac{\alpha_k}{\beta_k}\right)^{M}\left(1+\frac{\alpha_d}{\beta_d}\right)^{N}-1} - N \frac{\left(\frac{\alpha_d}{\beta_d}\right)\left(1+\frac{\alpha_d}{\beta_d}\right)^{N-1}\left(1+\frac{\alpha_k}{\beta_k}\right)^{M}}{\left(1+\frac{\alpha_d}{\beta_d}\right)^{N}\left(1+\frac{\alpha_k}{\beta_k}\right)^{M}-1} \right] \tag{4.17}$$

In the limit of $N, M \gg 1$, this expression reduces to

$$V = V_0 \left[M \frac{\left(\frac{\alpha_k}{\beta_k}\right)}{\left(1+\frac{\alpha_k}{\beta_k}\right)} - N \frac{\left(\frac{\alpha_d}{\beta_d}\right)}{\left(1+\frac{\alpha_d}{\beta_d}\right)} \right], \tag{4.18}$$

which in terms of the duty ratio of single kinesin Q_k and single dyenin Q_d is simply

$$V = V_0 \left[MQ_k - NQ_d \right] \tag{4.19}$$

Fig. 4.8 shows the variation of the average velocity of the bound vesicle with changes in the number of kinesin motors carried by the vesicle for different binding rate constants. Changing the relative rate of binding of each type of motor leads to a crossover from a net minus (-) end directed run of the vesicle to a (+) end directed run.

4.4.4 Mean first passage time

Mean first passage time is the typical time in which a bound vesicle detaches from the filament. In the steady state, the effective binding rate and unbinding rate are related by,

$$\beta_{eff}(1-P_{00}) = \alpha_{eff}P_{00} \tag{4.20}$$

Since the effective binding rate of the motors is simply $\alpha_{01} + \alpha_{10}$, we have

$$\beta_{eff} = \frac{P_{00}(\alpha_{01}+\alpha_{10})}{1-P_{00}} \tag{4.21}$$

The mean first passage time (T_m) to be detached from a bound state of the motor is simply $\frac{1}{\beta_{eff}}$ [26]. thus,

$$T_m = \frac{1}{\alpha_d+\alpha_k}\left[\left[\frac{1}{N}\left(1+\frac{\alpha_d}{\beta_d}\right)^{N}-1\right]+\left[\frac{1}{M}\left(1+\frac{\alpha_k}{\beta_k}\right)^{M}-1\right] + \frac{1}{MN}\left[\left(1+\frac{\alpha_d}{\beta_d}\right)^{N}-1\right]\left[\left(1+\frac{\alpha_k}{\beta_k}\right)^{M}-1\right]\right] \tag{4.22}$$

For the limit of $N, M \gg 1$ and $\frac{\alpha}{\beta} \gg 1$ we have,

$$T_m = \frac{\left(1+\frac{\alpha_d}{\beta_d}\right)^N \left(1+\frac{\alpha_k}{\beta_k}\right)^M}{MN(\alpha_d+\alpha_k)} = \frac{(1-Q_d)^{-N}(1-Q_k)^{-M}}{MN(\alpha_d+\alpha_k)} \tag{4.23}$$

So the first passage time for the detachment of the vesicle from the microtubule track increases rapidly with number of dyenin (N) and kinesin (M) bound to the vesicles.

4.4.5 Reversal time of vesicles

Transport quantity which can be easily measured in tracking experiments is the distribution of reversal times of the vesicle. By reversal time we mean the time in which a bound vesicle, moving in a specific direction(i.e., towards the plus-end or minus-end) reverses its direction. Solving the master equation using a Monte-Carlo simulation, two features emerge:

1. Increasing the number of docking sites of motors, i.e., N, M, leads to a increase in the reversal time. This means that one can achieve long distance directed walks by increasing N, M.

2. Regulating the binding rates affects the reversal time of the vesicle, such that when the relative difference between the binding rate constants of dyenin and kinesin motors increases, it leads to increase in the typical reversal time of the vesicle cargo. Conversely when the rate constants are roughly the same, the frequency of reversal increases and no net transport of vesicles is achieved.

Fig. 4.9 shows the distribution of the reversal time of the vesicle, when the rate constant of kinesin is very high ($\frac{\alpha_k}{\beta_k} = 5$) compared to dyenin ($\frac{\alpha_d}{\beta_d} = 0.2$). The plots are obtained for different number of motors attached to the vesicle cargo. Fig. 4.10 shows the semi-log plot of the same distributions. From it we infer that beyond $N = 3, M = 3$, the typical reversal time increases sharply. Correspondingly the mean reversal time also progressively increases. It is $1.9s, 3.8s, 9.0s, 17s, 29.8s$ for $(N = 2, M = 2)$, $(N = 3, M = 3)$, $(N = 4, M = 4)$, $(N = 5, M = 5)$ and $(N = 6, M = 6)$ respectively. Increasing the binding rate constant of dyenin from ($\frac{\alpha_d}{\beta_d} = 0.2$) to ($\frac{\alpha_d}{\beta_d} = 0.5$) and keeping the kinesin binding rate constant the same results in a sharp fall in the mean reversal time, (Fig. 4.11, 4.12). For instance the mean reversal time reduces more than 6 fold to 4.7 s.

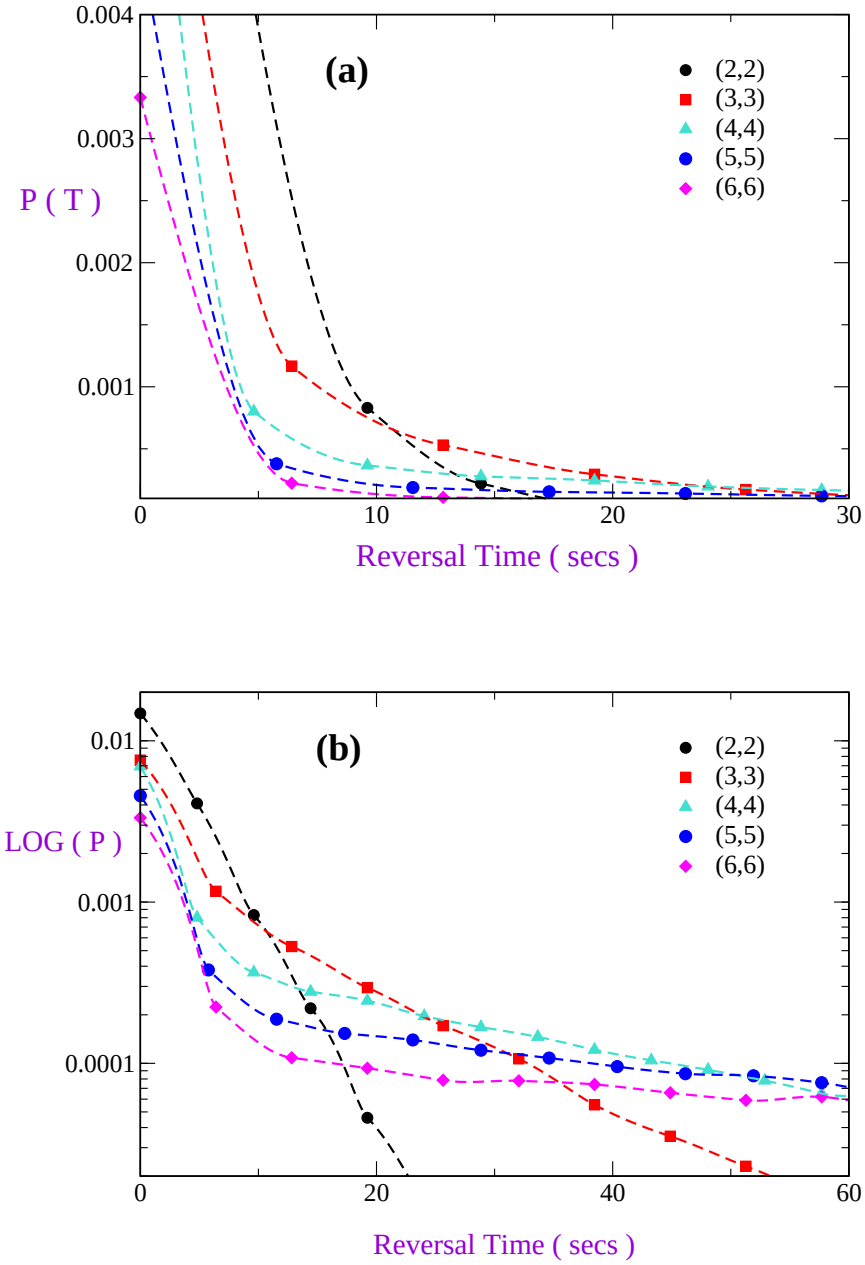

Figure 4.9: (a) Probability distribution of reversal times for vesicles pulled by dyenin and kinesin motors with different number of motors bound to the vesicles. $\frac{\alpha_d}{\beta_d} = 0.2$ and $\frac{\alpha_k}{\beta_k} = 5$ The values of N, M are respectively $(2, 2), (3, 3), (4, 4), (5, 5), (6, 6)$. (b) Probability distribution of reversal times in semi logscale for same parameter values as (a). Note that for $N \geq 4$, $M \geq 4$, the weight remains nearly constant, implying long directed runs.

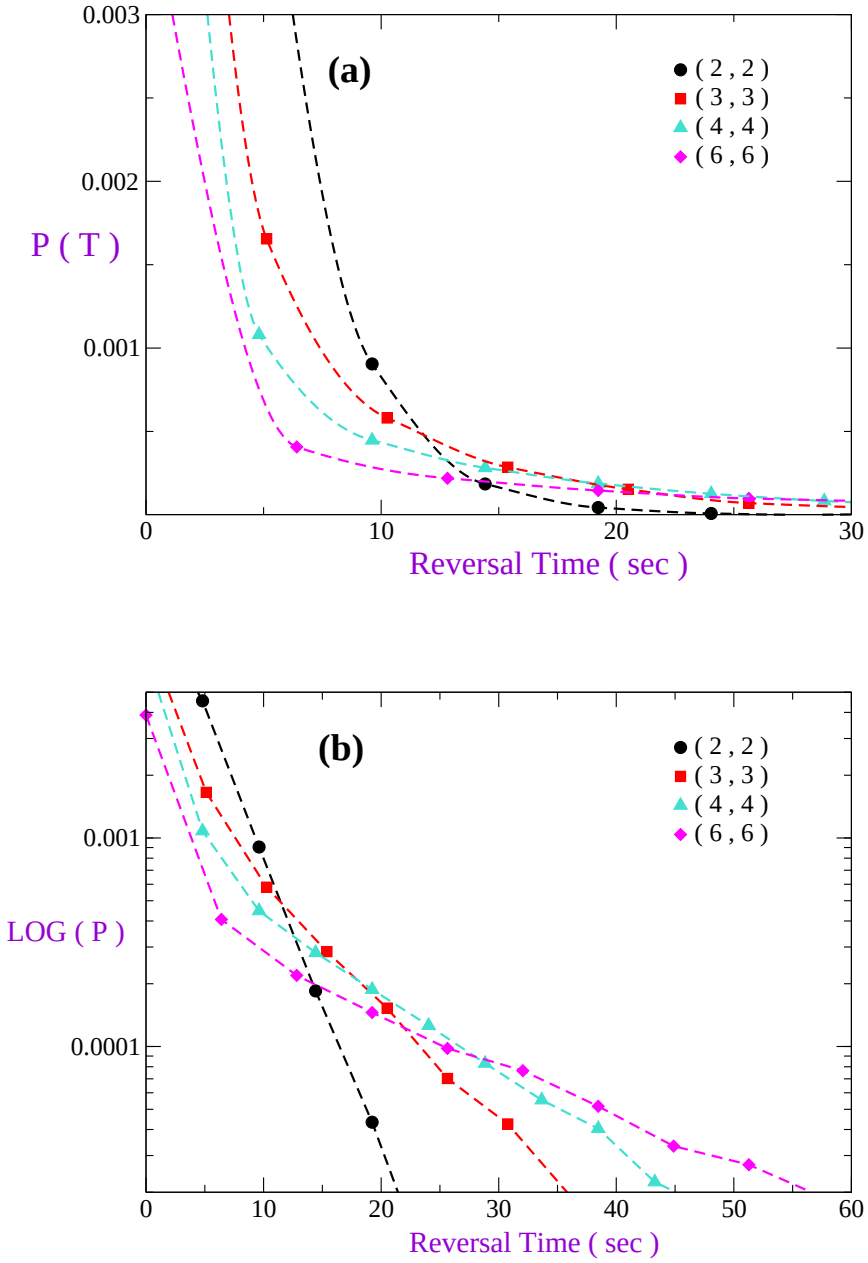

Figure 4.10: (a) Probability distribution of reversal times for vesicles pulled by dyenin and kinesin motors with different number of motors bound to the vesicles. $\frac{\alpha_d}{\beta_d} = 0.5$ and $\frac{\alpha_k}{\beta_k} = 5$. The values of (N, M) are respectively $(2, 2), (3, 3), (4, 4), (6, 6)$. (b) Probability distribution of reversal times in semi logscale for same parameter values as in (a). Note that increasing the binding rate constant of dyenin from 0.2 to 0.5 reduces the mean reversal time of the vesicle.

4.5 Conclusions

We have seen how long distance directed transport and regulation of cellular cargo transport is explained naturally within this simple transport model. Further various transport properties like distribution of bound motors, distribution of the velocity of the vesicle cargoes, the statistics of direction reversals of the cargoes are obtained within this framework. These quantities can be compared to statistical analysis of vesicle trajectories in melanophore cell or cell extracts. By making detailed comparison with various microscopic models of velocity and regulation, we hope to be able to fix the microscopic models.

In future we would like to study the distortion of the membrane bound organelles under the influence of the two oppositely directed motors.

Bibliography

[1] J. Howard, in *Mechanics of Motor Proteins and Cytoskeleton* (Sinauer Associates, Massachusetts, 2001).

[2] M.A. Welte, Curr. Biol. **14**, R525 (2004).

[3] R. Mallik and S. P. Gross, Curr. Biol. **14**, R971 (2004).

[4] P. Nelson, in *Biological Physics*, (W. H. Freeman and Company, New York, 2004).

[5] D. Bray, in *Cell Movements* (Garland Publishing, New York, 2001, 2nd ed).

[6] B. Alberts et al., in *Molecular Biology of the Cell* (Garland Science, New York, 2002, 4th ed).

[7] J. Howard, A. J. Hudspeth and R. D. Vale, Nature **342**, 154 (1989).

[8] R. Mallik, D. Petrov, S. A. Lex, S. J. King and S. P. Gross, Curr. Biol. **15**, 2075 (2005).

[9] J. T. Finer, R. M. Simmons and J. A. Spudich, Nature **368**, 113 (1994).

[10] A. D. Mehta, R. S. Rock, M. Rief, J.A. Spudich, M.S. Mooseker and R.E. Cheney, Nature **400**, 590 (1999).

[11] V. Levi, A. S. Serpinskaya, E. Gratton and V. Gelfand, Biophys. J. **90**, 318 (2006).

[12] R. H. Miller and R. J. Lasek, J. Cell. Biol. **101**, 2181 (1985).

[13] S.P. Gross, M.A. Welte, S.M. Block and E.F. Wieschaus, J. Cell. Biol. **156**, 715 (2002).

[14] R. D. Vale and R. A. Milligan, Science **288**, 88 (2000).

[15] A. Yildiz, M. Tomishige, R. D. Vale and P. R. Selvin, Science **303**, 676 (2004).

[16] R. Mallik, J. B. Udgaonkar and G. Krishnamoorthy, Proc. Indian. Acad. Sci. (Chem. Sci.) **115**, 307 (2003).

[17] A. A. Nascimento, J. T. Roland and V. I. Gelfand, Annu. Rev. Dev. Biol. **19**, 469 (2003).

[18] V. I. Rodionov, A. J. Hope, T. M. Svitkina and G. G. Borisy , Curr. Biol. **8**, 165 (1998).

[19] R. L. Morris and P. J. Hollenbeck, J. Cell. Sc. **104**, 917 (1993).

[20] S. R. Chada and P.J. Hollenbeck, J. Exp. Biol. **206** 1985 (2003).

[21] P.J. Hollenbeck, Front. Biosci. **1** d91 (1996).

[22] J. W. Murray, E. Bananis, A. W. Wolkoff, Mol. Biol. Cell. **11**, 419 (2000).

[23] V. I. Rodionov, J. Yi, A. Kashina, A. Oladpido and S. P. Gross, Curr. Biol. **13**, 1837 (2003).

[24] S. P. Gross, M. C. Tuma, S. W. Deacon, A. S. Serpinskaya, A. R. Reilein and V. Gelfand, J. Cell. Biol. **156**, 855 (2002).

[25] J. H. Hayden, Cell. Motil. Cytoskeleton. **10**, 255 (1988).

[26] S. Klumpp and R. Lipowsky, Proc. Natl. Acad. Sci. **102**, 17284 (2005).

[27] C. Leduc, O. Campas, K. B. Zeldovich, A. Roux, P. Jolimaitre, L. Bourel-Bonnet, B. Goud, J.-F. Joanny, P. Bassereau and J. Prost, Proc. Natl. Acad. Sci. **101**, 17096 (2004).

[28] S. M. Block, L. S. B Goldstein and B. J. Schnapp, Nature **348**, 348 (1990).

[29] R. D. Vale, T. Fanatsu, D. W. Pierce, L. Romberg, Y. Harada and T. Yanagida, Nature **380**, 451 (1996).

[30] H. Sakakibara, H. Kojima, Y. Sakai, E. Katayama and K. Oiwa, Nature **400**, 586 (1999).

[31] The binding rate for single dyenin motor is estimated by using the value of duty ratio quoted in [30].